Biosensors and Bioelectronics 141 (2019) 111406

Contents lists available at ScienceDirect

Biosensors and Bioelectronics

journal homepage: www.elsevier.com/locate/bios

A highly sensitive label-free electrochemical immunosensor based on poly (indole-5-carboxylicacid) with ultra-high redox stability

Taotao Yang[a,b], Xiaoning Ren[a,b], Ming Yang[a,b], Xing Li[a], Kaikai He[a], Ai Rao[a,b], Ying Wan[a,b], Hai Yang[a,b], Shenqi Wang[a], Zhiqiang Luo[a,b,*]

[a] College of Life Science and Technology, Huazhong University of Science and Technology, Wuhan 430074, China
[b] National Engineering Research Center for Nanomedicine, Huazhong University of Science and Technology, Wuhan 430074, China

ARTICLE INFO

Keywords:
Electrochemical immunosensor
Poly(indole-5-carboxylic acid)
Redox stability

ABSTRACT

The high stability of redox signal is one of the most crucial factors in construction of electrochemical immunosensors. However, the redox-active species usually show low stability and poor conductivity, which inhibits their application in electrochemical immunosensors. In this work, we report that the conductive polymer poly(indole-5-carboxylic acid) (PIn-5-COOH) possesses ultra-high redox stability. The redox signal of PIn-5-COOH could remain 96.03% after 500 cyclic voltammery (CV) cycles in buffer solution with pH of 6.2, while the redox signals in most of the previous reports only remained less than 90% after 50 CV cycles. Our mechanism investigation indicated that the ultra-high redox stability of PIn-5-COOH should be attributed to its stable structure. The electrochemical immunosensors fabricated with PIn-5-COOH/MWCNTs-COOH nanocomposite showed a wide linear range from 0.001 ng mL^{-1} to 100 ng mL^{-1} and a low detection limit of 0.33 pg mL^{-1} for the detection of alpha fetoprotein. This study opens up a new avenue for the construction of electrochemical immunosensors with ultra-stable redox signal.

1. Introduction

The electrochemical immunosensor has attracted extensive interests in recent years due to its advantages of high sensitivity, high specificity, easy operation, simple instrumentation and miniaturization capability (Yang et al., 2017; Niu et al., 2017; Li et al., 2017; Zhang et al., 2018). Recently, the application of multiplexed electrochemical immunosensors in organ-on-a-chip system for real time electrochemical detection and monitory is an emerging research field (Jochen et al., 2018; Gao and Teng, 2016). For example, Zhang et al. reported the integration of electrochemical immunobiosensors with a human liver-cancer-and-heart-on-a-chip platform for drug screening and long-term monitoring of drug induced organ toxicity (Zhang et al., 2017). The electrochemical immunobiosensors provided the capability of real-time, in situ monitoring of soluble biomarkers such as albumin, glutathione S-transferase α (GST-α), creatine kinase MB (CK-MB) in microfluidic system. In this situation, continuous electrochemical measurements are demanded, and therefore stability of an electrochemical immunosensor is of a crucial importance for real time monitoring of the analytes of interest. Since electrochemical sensing is based on the measurement of electron transfer in a redox reaction, the stability of redox signal is of significant importance for construction of stable electrochemical immunosensors.

Various of redox-active species have been utilized in electrochemical immunosensors as electronic media, such as prussian blue (Hedieh et al., 2018; Dong et al., 2017), methylene blue (Zhang et al., 2012), ferrocene (Qiu et al., 2009), thionin (Zhai et al., 2016), toluidine blue (Wang et al., 2017) and nile blue (Ali et al., 2015). However these redox-active species usually show poor stability and low conductivity, and exploring novel methods to improve the stability and conductivity of redox-active species is a hot research topic. For instance, Li et al. reported a double protection method in which polyaniline and multi-walled carbon nanotubes were used to make nanocomposite with prussian blue, and the cathodic current remained 93.97% after 50 continuous cyclic voltammery (CV) cycles (Li et al., 2015). Zhang et al. synthesized a redox-stable nanocomposite through π-π interaction between graphene and methylene blue. The oxidation peak current and reduction peak current remained 88.81% and 90.17% of the initial value after 100 continuous CV cycles, respectively (Zhang et al., 2012). Qiu et al. proposed to covalently graft ferrocene onto the chitosan long chain (Qiu et al., 2009). The redox stability of ferrocene was improved through preventing the leakage of ferrocene from the matrix. Although

* Corresponding author. College of Life Science and Technology, Huazhong University of Science and Technology, Wuhan 430074, China.
E-mail address: zhiqiangluo@hust.edu.cn (Z. Luo).

https://doi.org/10.1016/j.bios.2019.111406
Received 18 March 2019; Received in revised form 21 May 2019; Accepted 1 June 2019
Available online 06 June 2019
0956-5663/

these nanocomposite methods can be used to improve the stability of redox-active species in some extent, fabricating electrochemical immunosensors with highly stable redox signal remains a huge challenge.

Redox-active conducting polymers have attracted many interests for their application in electrochemical sensors, electrocatalysts, supercapacitors and batteries (Song and Palmore, 2006; Maciejewska et al., 2011; Luo et al., 2012; Zhao et al., 2013; Xu et al., 2014; Utkarsh et al., 2017; Elena et al., 2018). Particularly, conducting polymer polyindole derivatives show great potential in electrochemical immunosensor application due to their distinguished advantages such as good conductivity, abundant functional groups, high redox activity, and excellent biocompatibility (Li et al., 2008; Kashish et al., 2015; Zhang, 2016). However, the redox stability of polyindole derivatives had never been discussed. Most of works just utilized conducting polyindole derivatives for immobilization application in electrochemical sensors while there are very few of works reported on the application of redox-active polyindole derivatives in electrochemical sensors. Take the redox-active poly(indole-5-carboxylic acid) (PIn-5-COOH) as an example, to date, there are only two papers reported the application of redox signal of PIn-5-COOH in electrochemical sensors. Li developed a DNA electrochemical sensor based on electrochemical polymerization of PIn-5-COOH on the glassy carbon electrode. The label-free DNA sensors based on PIn-5-COOH displayed a linear range from 3.34×10^{-9} to 1.06×10^{-8} mol L^{-1} and a detection limit of 1.0×10^{-9} mol L^{-1} (Li et al., 2008). Zhang constructed a DNA electrochemical sensor based on ZnO/PIn-5-COOH nanocomposite. The linear range for electrochemical DNA hybridization detection was from 1.0×10^{-15} to 1.0×10^{-9} mol L^{-1}, and the detection limit was as low as 2.2×10^{-16} mol L^{-1} (Zhang, 2016).

Herein, we systematically investigated the redox stability of PIn-5-COOH prepared by a facile chemical polymerization method and found that PIn-5-COOH possessed ultra-high redox stability. The retention rate of the reduction peak current of PIn-5-COOH is 99.79% after 100 continuous CV cycles and 96.03% even after 500 continuous CV cycles in buffer solution. While the redox signals in most of the previous works only remained less than 90% after 50 CV cycles. Our mechanism study indicated that the ultra-high redox stability of PIn-5-COOH should be attributed to its stable structure. As a demonstration of the capability of PIn-5-COOH in immunosensor application, alpha fetoprotein (AFP) was chosen as a model biomarker for label-free electrochemical immunosensors, which were constructed on basis of PIn-5-COOH/MWCNTs-COOH nanocomposite. The electrochemical immunoassays for AFP demonstrated a wide linear range from 0.001 ng mL^{-1} to 100 ng mL^{-1} and a low detection limit of 0.33 pg mL^{-1}. The fabricated immunosensor exhibits good selectivity, reproducibility, and shows great potential for application in clinical sample analysis. This study opens up a new avenue for the construction of electrochemical biosensors with ultra-stable redox signal.

2. Experimental

2.1. Chemicals and materials

Alpha fetoprotein (AFP), anti-AFP antibody, bovine serum albumin (BSA) and other cancer biomarker were purchased from Bosai Biotechnology Co., Ltd. (Zhengzhou, China). Human serum samples were purchased from Guangzhou hongquan bio-tel. (Guangzhou, China). Dopamine, glucose, glycine, L-glutamate, ascorbic acid, EDC, NHS and MES were purchased from J&K Scientific Ltd. (Beijing China). MWCNTs-COOH samples were purchased from Nanjing Xian Feng Nanomaterials Technology Co., Ltd. (Nanjing, China). Indole-5-carboxylic acid (In-5-COOH) was purchased from Shanghai Vita Chemical Regent Co., Ltd. (Shanghai, China).

2.2. Synthesis of Poly(indole-5-carboxylic acid) (PIn-5-COOH)

The PIn-5-COOH was prepared by a facile chemical method. 100 mg indole-5-carboxylic acid monomer was dissolved in 2.5 mL ethanol (solution A), and 100 mg APS was dissolved in 10.0 mL H_2SO_4 solution (pH = 1.0) (solution B). Under uniform stirring, solution B was slowly added into solution A. The mixture was kept stirring for 6 h at room temperature. Finally, the products were centrifuged and washed with water and ethanol repeatedly. The PIn-5-COOH was dispersed in deionized water, and the concentration was estimated to be 0.2 mg mL^{-1}.

PIn-5-COOH/MWCNTs-COOH nanocomposite was prepared with the same solutions and process. MWCNTs-COOH (2 mg) was fully mixed with solution A before added solution B.

In order to investigated the mechanism of redox stability, the poly (5-formylindole) (PIn-5-CHO), poly(5-aminoindole) (PIn-5-NH_2), poly (5-fluoroindole) (PIn-5-F) were also synthesized with the same method.

2.3. Fabrication of electrochemical immunosensors

PIn-5-COOH/MWCNTs-COOH dispersion (8 μL; 0.2 mg mL^{-1}) was dropped on the bare glass carbon electrode (GCE) and dried in infrared drying oven. Then the modified electrodes were immersed into mixing solution containing EDC (100 mM), NHS (40 mM) and MES (100 mM) for 12 h to activate the carboxyl group, and then washed with deionized water for twice. After that, 8 μL of anti-AFP antibody was dropped onto the modified electrode and incubated for 2 h at 37 °C. After being washed with PBS, 8 μL of BSA (1 mg mL^{-1}) was dropped onto the modified electrode for 30 min to block the residual active sites and then washed with deionized water. Finally, the immunosensor was obtained. The prepared BSA/anti-AFP/PIn-5-COOH/MWCNTs-COOH/GCE was stored in a 4 °C refrigerator when not use.

2.4. Apparatus and measurements

Fourier transform infrared (FT-IR) spectrum was collected with a Nicolet Magna-IR 750. Scanning electron microscope (SEM) images were investigated with a SU8020 scanning electron microscope. Transmission electron microscope (TEM) characterization was characterized on an electronic microscopy (HITACHI HT7700) operating at 100 kV. X-ray photoelectron spectroscopy (XPS) measurements were performed on an Escalab 250Xi system, using nonmonochromatic Al Ka radiation. The electrochemical properties measurements were carried out on a CHI660E electrochemical workstation (Shanghai Chenhua Apparatus Corporation, China) with a standard three-electrode system. A platinum sheet electrode (5 mm × 5 mm) was used as the counter electrode, a saturated calomel reference electrode (SCE) was used as the reference electrode, and a bare GCE (Φ = 3 mm) was used as the working electrode.

3. Results and discussion

3.1. Characterization of the PIn-5-COOH and its nanocomposite

FT-IR spectra of the In-5-COOH monomer and PIn-5-COOH polymer were recorded to study the polymerization mechanism. The absorption peaks in the spectra of the PIn-5-COOH (Fig. 1A(b)) were obviously broadened in comparison with that of In-5-COOH monomer (Fig. 1A(a)), which may be attributable to the wide conjugated chain length distribution of polymers (Hu et al., 2016; Liu et al., 2016). The peaks between 710 cm^{-1} and 825 cm^{-1} in the spectra of In-5-COOH monomer and PIn-5-COOH polymer were assigned to the three adjacent C–H deformation vibration of ring hydrogens on benzenic ring, which suggested that benzene ring were 1,2,3-trisubstitution (Ma et al., 2015). The = CH–N stretching appeared at 894 cm^{-1} for In-5-COOH monomer, while this vibration disappeared in the PIn-5-COOH (Liu

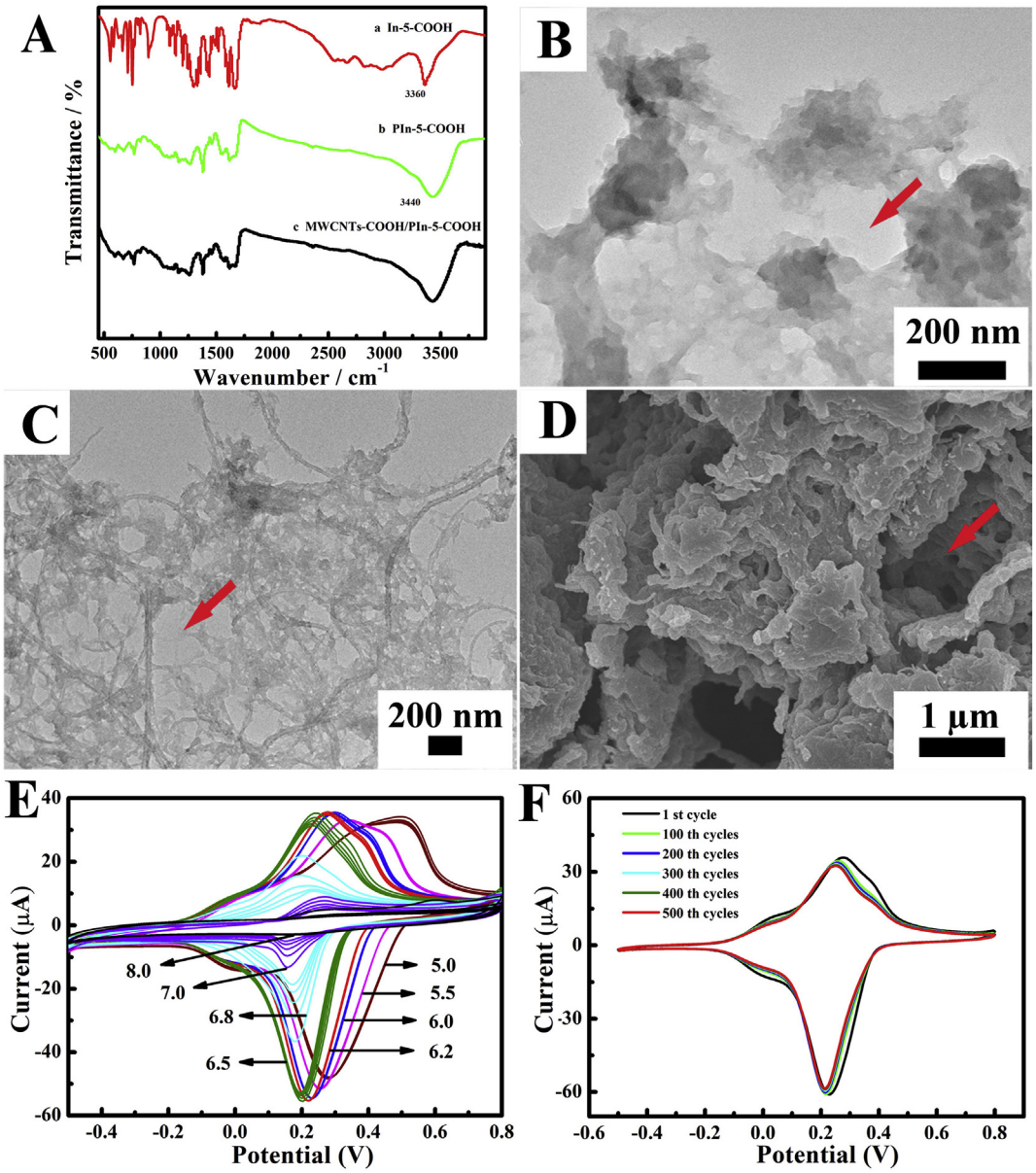

Fig. 1. The characterization of PIn-5-COOH and PIn-5-COOH/MWCNTs-COOH nanocomposite. (A) FT-IR spectra of In-5-COOH, PIn-5-COOH and PIn-5-COOH/MWCNTs-COOH nanocomposite. TEM images of PIn-5-COOH (B), PIn-5-COOH/MWCNTs-COOH nanocomposite (C), and SEM image of PIn-5-COOH/MWCNTs-COOH nanocomposite (D). (E) Influences of pH on the redox activity of PIn-5-COOH. (F) Cyclic voltammograms (CVs) study of redox stability of PIn-5-COOH. (Up to 500 CV cycles of PIn-5-COOH/GCE were measured in 0.1 M PBS with pH of 6.2 and scan rate of 100 mV s^{-1})

et al., 2016). The C–H vibration peak of the pyrrole ring located at approximately 3003 cm^{-1} for In-5-COOH monomer and disappeared for PIn-5-COOH. The absorption bands at 1132 cm^{-1} and 3360 cm^{-1} originated from the vibration modes of C–N and N–H on the pyrrole ring, respectively (Nidhi et al., 2011; Mike et al., 2017; Leela et al., 2010). These results indicated that the polymerization should happen at the 2 and 3 positions. Compared with FT-IR spectrum of PIn-5-COOH, the FT-IR spectrum of PIn-5-COOH/MWCNTs-COOH nanocomposite (Fig. 1A(c)) showed a little positive shift of the C=C bond, which should be attributed to the π-π interaction between PIn-5-COOH and MWCNTs-COOH.

The morphology features of the chemical polymerized PIn-5-COOH and the as-synthesized PIn-5-COOH/MWCNTs-COOH nanocomposite were investigated by TEM and SEM. The TEM image of PIn-5-COOH (Fig. 1B) showed the 3D hierarchical porous structure, which could not only provide the favorable microenvironment, large surface area, but also could promote direct electron transfer. Fig. 1C showed the TEM image of PIn-5-COOH/MWCNTs-COOH nanocomposite. It can be seen that the PIn-5-COOH wrapped on the MWCNTs-COOH, and formed 3D porous structure and connection, which would offer great surface area for bonding of biomarkers. The SEM image (Fig. 1D) revealed that PIn-5-COOH/MWCNTs-COOH nanocomposite formed a 3D hierarchical porous structure, which would benefit the analytical performance of PIn-5-COOH/MWCNTs-COOH based electrochemical sensors.

The cyclic voltammograms (CVs) were performed to reveal the electrochemical behaviors of PIn-5-COOH (Fig. 1E). The CVs of PIn-5-COOH were measured in 0.1 M PBS with different pH values ranging from 5.0 to 8.0, and the redox activity of PIn-5-COOH reached a maximum around pH of 6.2. The redox signal stability of PIn-5-COOH was subsequently investigated in 0.1 M PBS of pH 6.2. Fig. 1F displayed CVs (1st, 100th, 200th, 300th, 400th and 500th cycles) of PIn-5-COOH/GCE with a scan rate of 100 mV s^{-1}. The cathodic current was 60.94 μA at the first cycle and the retention rate of the cathodic current was 99.79% after 100 consecutive cycles. After consecutive 500 CV

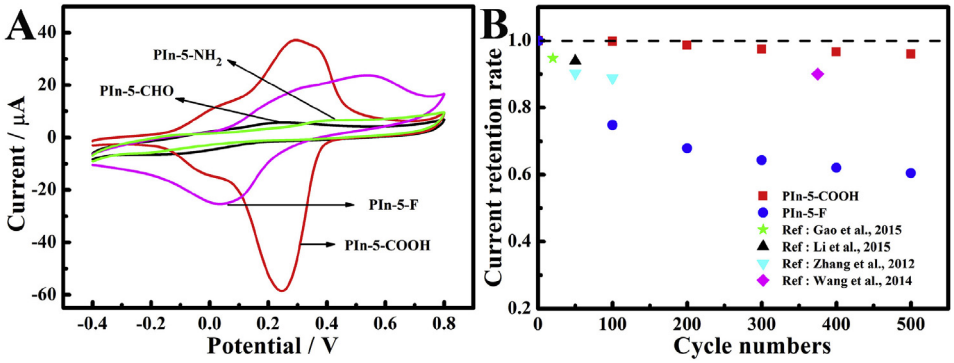

Fig. 2. Comparison of redox stability of PIn-5-COOH with those of other redox-active species. (A) Effect of functional groups in PIn derivatives on the redox activity. (B) Redox stability of PIn-5-COOH, PIn-5-F, and other reported redox-active species.

cycles, the cathodic current still remained 96.03%. To the best of our knowledge, the redox stability of PIn-5-COOH is superior to those of any reported redox-active species used for electrochemical sensor application.

3.2. Mechanism study of PIn-5-COOH with ultra-high redox stability

In order to compare redox stability of PIn-5-COOH with those of other redox-active species, the redox properties of other PIn derivatives, such as PIn-5-F, PIn-5-CHO, and PIn-5-NH_2, were studied. Fig. 2A showed their typical CVs measured in 0.1 M PBS with pH of 6.2. A couple of redox peaks can be observed in the CVs of PIn-5-COOH and PIn-5-F, while there was a very small redox peak in the CV of PIn-5-CHO and almost no redox peak in the CV of PIn-5-NH_2. The CVs of PIn-5-F, PIn-5-CHO, and PIn-5-NH_2 were also measured in 0.1 M PBS with different pH value ranging from 5.0 to 8.0 to assess the optimized pH for each (Fig. S1). Even with optimized pH, redox activity of PIn-5-CHO and PIn-5-NH_2 were still too weak for electrochemical sensor application. Both PIn-5-COOH and PIn-5-F had apparent redox signals, and showed promise as redox-active species for electrochemical sensors. To understand the origin of difference in redox activity of PIn derivatives, quantum chemistry calculation of PIn derivatives is demanded in future work.

The redox signal stability of PIn-5-COOH with a function of CV cycling numbers was illustrated in Fig. 2B. For comparison, the redox signal stability of several previous reports were also illustrated in Fig. 2B (Zhang et al., 2012; Wang et al., 2014; Gao et al., 2015; Li et al., 2015). Only a few works reported the redox stability study with CV cycling numbers more than 50, and the redox signals in most of the previous works remained less than 90% after 50 CV cycles. As for the redox signal stability of PIn-5-F, after consecutive 500 CV cycles the retention rate of the cathodic current at pH 5.5 and pH 6.2 were 60.5% and 54.8%, respectively (see Fig. 2B and Fig. S2). Therefore, it is conclusive that PIn-5-COOH had much higher redox stability when compared with other redox-active species.

To understand the mechanism associated with the redox stability of PIn derivatives, the electrochemical impedance spectra (EIS), FT-IR and XPS of PIn-5-COOH and PIn-5-F were investigated before and after 500 consecutive CV cycling which were performed in 0.1 M PBS with pH of 6.2. Fig. 3A and Fig. 3B showed the typical Nyquist plots of PIn-5-COOH/GCE and PIn-5-F/GCE in 0.1 M KCl containing 5.0 mM $K_3Fe(CN)_6/K_4Fe(CN)_6$ (1:1), respectively. The EIS of PIn-5-COOH/GCE displayed a small semicircle (R_{et} = 10 Ω), and the R_{et} had almost no change after CV cycling. While for PIn-5-F/GCE, initially the R_{et} had a larger value of 64 Ω, and the R_{et} further increased to 80 Ω after CV cycling. The EIS characterization indicated that in comparison with PIn-5-F, the conductivity, interface resistance, and electrical stability of PIn-5-COOH are much superior.

Fig. 3C showed FT-IR of PIn-5-COOH before and after CV cycling. As shown in Fig. 3C(a), the absorption bands at 3433, 1673, 1376, 1263 and 763 cm^{-1} could be attributed to N–H stretching, –COOH group, C–C stretching, C–N stretching, and C–H stretching, respectively (Ma et al., 2015; Nidhi et al., 2011; Leela et al., 2010). After CV cycling, the FT-IR of PIn-5-COOH almost had no change (Fig. 3C(b)), which indicated that PIn-5-COOH possessed a good structure stability. As for the FT-IR of PIn-5-F (Fig. 3D), the absorption bands at 1462, 1184 and 627 cm^{-1} were characteristic of fluoro groups (Yucel et al., 2004; Nie et al., 2007), which became weakened after CV cycling. Moreover, the peak at 3442 cm^{-1} which was the characteristic absorption of the N–H bond, shifted to 3455 cm^{-1} after CV cycling. These results indicated that the atomic structure of the PIn-5-F changed after CV cycling.

The XPS C1s core-level spectra for the PIn-5-COOH and PIn-5-F before and after CV cycling were shown in Fig. 3E and F, respectively. Through the Gaussian-Lorentzian fitting, these C1s spectra of PIn-5-COOH could be fitted into four peaks centered at binding energies (BE) of 284.6 eV (C–C/C═C), 285.3 eV (C═N), 286.6 eV (C–N/C–O) and 288.6 eV (C═O/O–C═O) (Heike et al., 2015; Mandira et al., 2017). After CV cycling, there was almost no change in the Gaussian-Lorentzian fitting, indicating no change in atomic bonding configurations of PIn-5-COOH. As shown in Figs. S3A and S3B, the N1s and O1s spectra also supported this result. For comparison, the C1s spectra of PIn-5-F were also investigated. The C1s spectra of PIn-5-F (Fig. 3F) can be fitted with four components: BE of 284.6 eV assigned to C–C/C═C, BE of 285.4 assigned to C═N, BE of 286.6 eV assigned to C–N/C–O, and BE of 288.6 eV assigned to C–F. After CV cycling, the peak intensity of C–F became weakened apparently, which might be caused by the broken of C–F bonds. Moreover, the F1s spectra (Fig. S3D) demonstrated a BE shift from 687.10 eV to 686.96 eV, which indicated that fluorine atom acquired more electrons from carbon atom after CV cycling. All the results of FT-IR and XPS investigation indicated that the redox stability of PIn derivatives is determined by their structure stability during CV cycling.

3.3. Construction and characterization of PIn-5-COOH based immunosensor

Fig. 4A illustrated the step-by-step construction process of electrochemical immunosensor based on PIn-5-COOH/MWCNTs-COOH nanocomposite. Fig. 4B showed CV of PIn-5-COOH/MWCNTs-COOH nanocomposite on GCE and CVs of each component for comparison. As shown in the inset of Fig. 4B, no redox peaks could be observed at bare GCE (inset a) and MWCNTs-COOH/GCE (inset b) in PBS. The CV of PIn-5-COOH/GCE showed a pair of redox peaks (Fig. 4B(c)), while the CV peak currents of PIn-5-COOH/MWCNTs-COOH nanocomposite on GCE increased significantly (Fig. 4B(d)). Electron transfer in PIn-5-COOH/MWCNTs-COOH nanocomposite was promoted since the MWCNTs-COOH had excellent conductivity. EIS was also used to investigate the conductivity and interface resistance of each component (Fig. 4C).

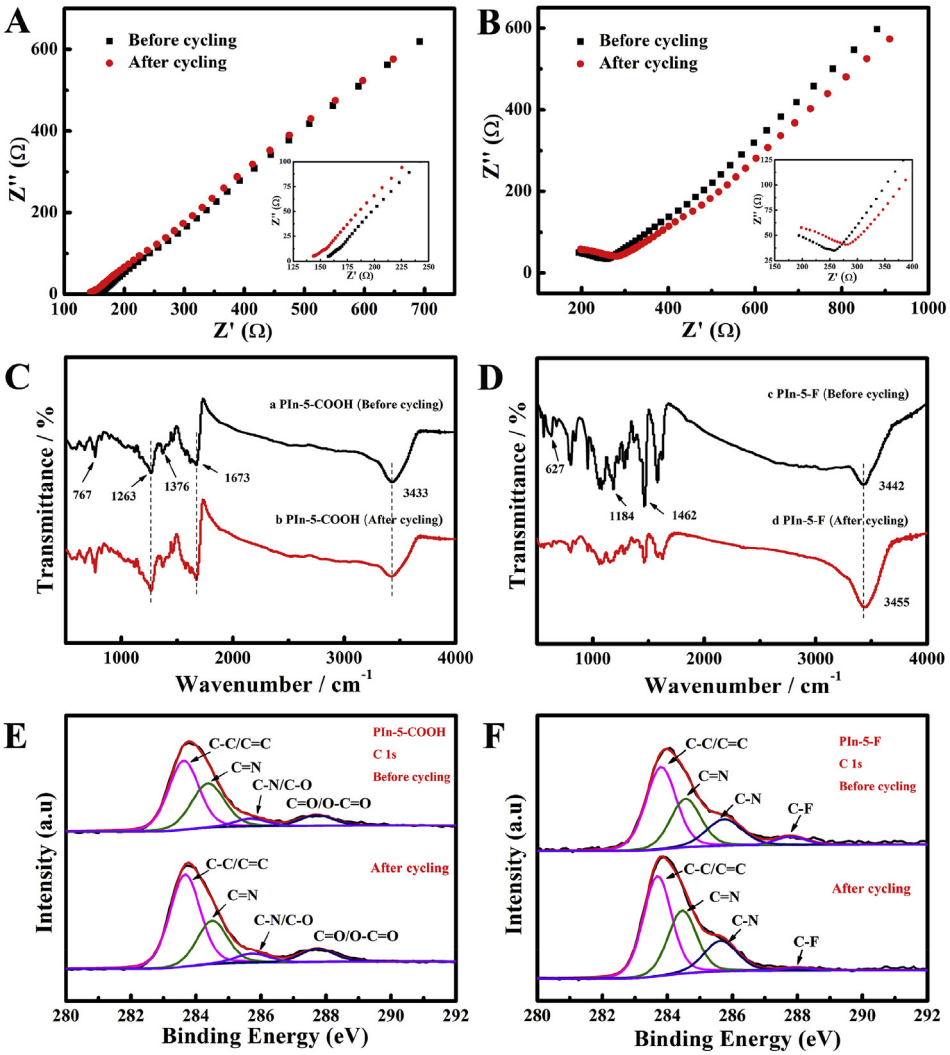

Fig. 3. The characterization of PIn derivatives before and after 500 CV cycling (the CV cycling were performed in 0.1 M PBS with pH of 6.2). The EIS of the PIn-5-COOH/GCE (A) and PIn-5-F/GCE (B) in the frequency range 0.1–10000 Hz. FT-IR spectra of PIn-5-COOH (C) and PIn-5-F (D). XPS C1s core-level spectra of PIn-5-COOH (E) and PIn-5-F (F).

Compared with EIS of bare GCE (curve a) which displayed a large semicircle, the EIS of MWCNTs-COOH/GCE (curve b), PIn-5-COOH/GCE (curve c) and PIn-5-COOH/MWCNTs-COOH/GCE (curve d) showed straight lines indicating good conductivity and small interface resistance. The PIn-5-COOH/MWCNTs-COOH nanocomposite with good redox activity and high conductivity would serve as an effective electrochemical immunosensor platform.

The electrochemical performance of sensor electrode after each step of fabrication process was monitored by DPV and EIS measurements. As shown in Fig. 4D, no peak current could be observed in DPV of bare GCE (curve a), while the DPV of PIn-5-COOH/MWCNTs-COOH/GCE displayed a remarkable peak current at the potential of 0.22 V (curve b). After anti-AFP immobilization onto PIn-5-COOH/MWCNTs-COOH/GCE, the redox peak current severely decreased, which indicated that the anti-AFP successfully bonded onto the surface of PIn-5-COOH/MWCNTs-COOH/GCE (curve c). And then, the redox peak current decreased again (curve d) after BSA was used to block non-specific sites. In final step, the peak current further decreased dramatically, because the AFP antigen was incubated to immunosensor to form insulating antigen-antibody complex (curve e). Fig. 4E showed the EIS of the electrode after each step of fabrication process. A small semicircle (R_{et} = 608 Ω) displayed at the EIS of bare GCE (curve a), while a straight line without semicircle was observed in the EIS of PIn-5-COOH/MWCNTs-COOH/GCE (curve b). After immobilization of anti-AFP antibodies, a semicircle appeared in EIS (curves c) and the R_{et} significantly increased to 1090 Ω since insulating antibodies layer inhibited electronic transfer. Subsequently, the nonspecific active sites have been blocked by BSA, and the R_{et} further increased to 2746 Ω (curve d). Finally, AFP was immobilized on the surface of BSA/anti-AFP/PIn-5-COOH/MWCNTs-COOH/GCE forms antigen-antibody complex, resulting in an increased R_{et} of 4184 Ω (curve e). All the DPV and EIS results confirmed that the immunosnesor had been successfully fabricated.

Prior to assess immunoassay performance of the PIn-5-COOH based immunosensor, the incubation time of antibody and antigen were carefully optimized. Fig. 5A showed the effects of incubation time of antibody on the analytical performance of immunosensors. The inhibition ratio increased from 60 min to 120 min, and decreased from 120 min to 180 min. Therefore, 120 min was chosen as the optimal incubation time for anti-AFP antibody. Fig. 5B displayed the inhibition ratio as a function of AFP incubation time, which indicated that the 150 min was the optimal incubation time for antigen. Under the optimized conditions, the fabricated immunosensors were incubated with different concentrations of AFP in deionized water. As shown in Fig. 5C, the peak current decreased gradually with the incremental AFP concentrations. Fig. 5D showed a linear relationship of the inhibition ratio

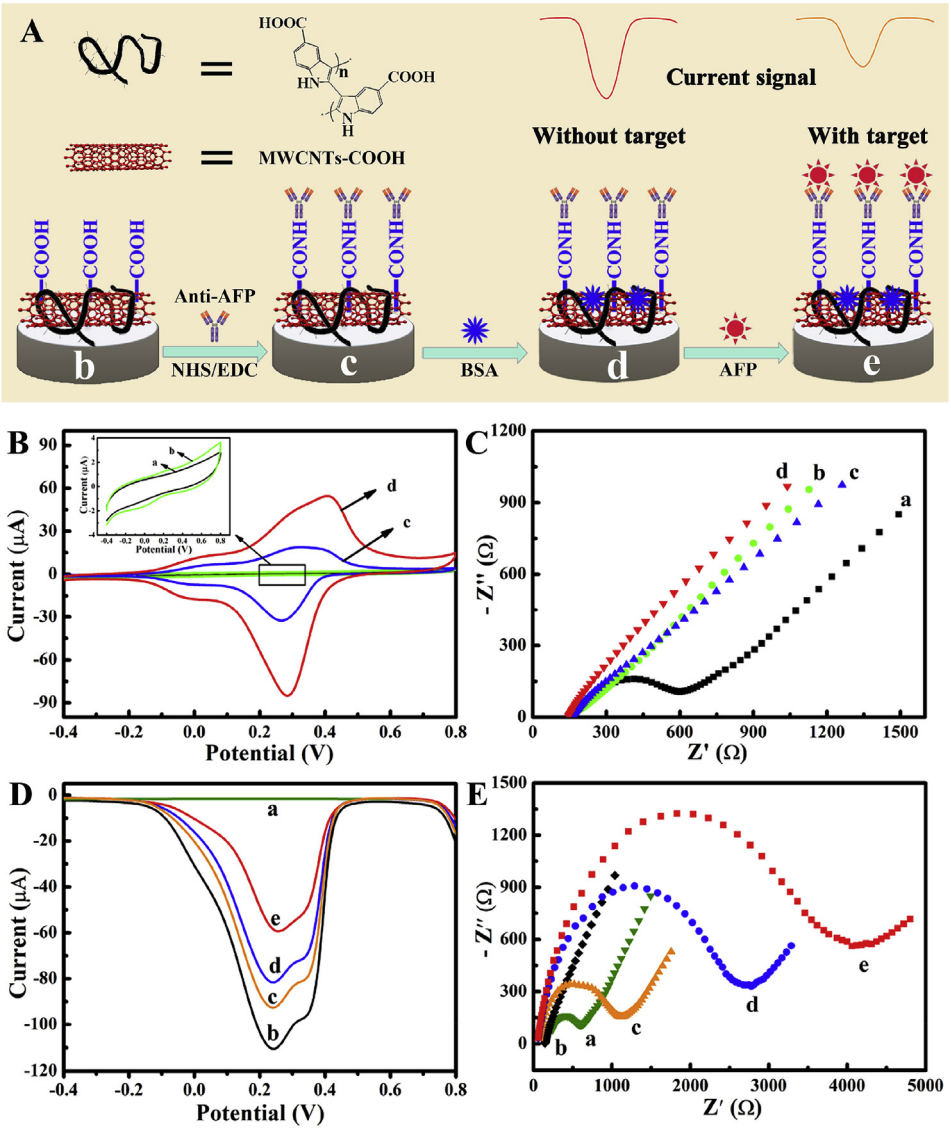

Fig. 4. The electrochemical characterization of PIn-5-COOH based immunosensor. (A) Schematic illustration of the fabrication procedure of the immunosensor. (B) CVs and (C) EIS of bare GCE (a), MWCNTs-COOH/GCE (b), PIn-5-COOH/GCE (c) and PIn-5-COOH/MWCNTs-COOH/GCE (d). (D) DPVs and (E) EIS of bare GCE (a), PIn-5-COOH/MWCNTs-COOH/GCE (b), anti-AFP/PIn-5-COOH/MWCNTs-COOH/GCE (c), BSA/anti-AFP/PIn-5-COOH/MWCNTs-COOH/GCE (d) and modified GCE after incubation with 1 ng mL^{-1} AFP (e). CVs and DPVs: 0.1 M PBS (pH 6.2) at a scan rate of 100 mV s^{-1}. EIS: 5.0 mM $K_3Fe(CN)_6/K_4Fe(CN)_6$ (1:1) containing 0.1 M KCl, and the frequency range was 0.1–10000 Hz with signal amplitude of 0.5 mV.

of current response with the concentration of AFP. The linear regression equation could expressed as $(I_0–I)/I_0 = 0.1218\lg C_{AFP} + 0.4460$, and the linear range was from 0.001 to 100 ng mL^{-1} ($R^2 = 0.9920$; n = 5). The detection limit was estimated to be 0.33 pg mL^{-1} (S/N = 3). It should be pointed out that without combination with MWCNTs-COOH, the detection limit of BSA/anti-AFP/PIn-5-COOH/GCE immunosensor is around 3.3 pg mL^{-1}, one order of magnitude higher (as shown in Fig. S4). The MWCNTs-COOH in nanocomposite would benefit the analytical performance of PIn-5-COOH/MWCNTs-COOH based electrochemical sensors due to enhanced conductivity and surface area of nanocomposite. The BSA/anti-AFP/PIn-5-COOH/MWCNTs-COOH/GCE immunosensors were further tested with human serum samples. As shown in Fig. S5, the linear range was from 0.001 to 100 ng mL^{-1} and the estimated detection limit was about 0.33 pg mL^{-1}.

The selectivity, repeatability and stability of immunosensors are important factors in electrochemical analysis of clinical biomarkers. In order to investigate the specificity of the BSA/anti-AFP/PIn-5-COOH/MWCNTs-COOH/GCE immunosensor, several substrates were chosen for control experiments in both deionized water and human serum samples, (Fig. 5E and Fig. S6). Although the concentration of interfering substances was 50 times or 10000 times higher than the concentration of AFP, the interfering substances inhibition ratio was much lower than AFP. These results suggested that the proposed immunosensor had a good specificity for AFP. To investigate the repeatability of the BSA/anti-AFP/PIn-5-COOH/MWCNTs-COOH/GCE immunosensor, five fresh immunosensors were prepared through the same procedure for the detection of AFP (8 μL, 1 ng mL^{-1}). The relative standard deviation (RSD) of the five measurements was 4.7%, indicating acceptable fabrication reproducibility. The redox signal stability of final assembled BSA/anti-AFP/PIn-5-COOH/MWCNTs-COOH/GCE immunosensor was investigated and the 1st, 100th, 200th, 300th, 400th and 500th CV cycles of assembled immunosensors were displayed in Fig. S7. The retention rate of the cathodic current was 96.04% after 100 consecutive cycles and 92.01% after 500 consecutive cycles. Table S1 showed the comparison of immunoassay performance of the proposed immunosensor with previously reported electrochemical immunosensors. It was indicated that our proposed immunosensor showed great advantage in redox signal stability and their performance in selectivity, linear range and detection limit were among the best. The storage stability of the immunosensor was also investigated (Fig. 5F). Five immunosensors were stored in PBS (pH = 6.2) at 4 °C, and measured every 5 days. The current response retained 97.30% and 88.21% of its initial current after 15 days and 30 days, respectively, which indicated that the immunosensors had acceptable long term stability. To evaluate practicability of the immunosensors in real sample detection, the recovery experiments were performed by standard addition methods in

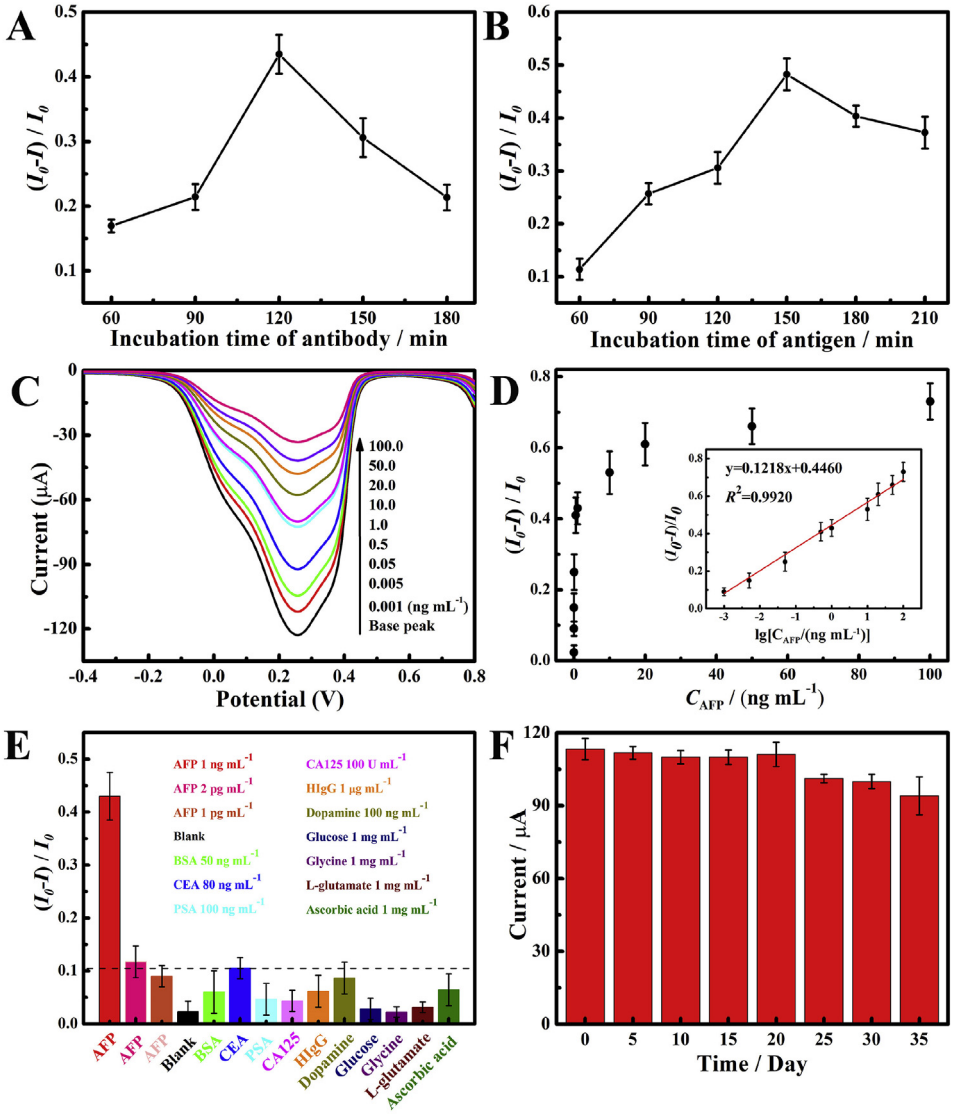

Fig. 5. The immunoassay performance of PIn-5-COOH based immunosensor. Effects of (A) incubation time of antibody (9.323 μg mL^{-1}) and (B) incubation time of antigen (10 ng mL^{-1}) on the analytical performance of immunosensors. (C) DPV of the immunosensor after being incubated with different concentrations of AFP (0.001, 0.005, 0.05, 0.5, 1.0, 10.0, 20.0, 50.0 and 100 ng mL^{-1}). (D) Calibration curve for AFP determination. (Inset) Linear plot of the inhibition ratio as a function of logarithmic concentration of AFP. (E) Comparison of the response of the immunosensor to 1 ng mL^{-1} AFP, 50 ng mL^{-1} BSA, 80 ng mL^{-1} CEA, 100 ng mL^{-1} PSA, 100 U mL^{-1} CA125, 1 μg mL^{-1} HIgG, 100 ng mL^{-1} dopamine, 1 mg mL^{-1} glucose, glycine, L-glutamate and Ascorbic acid. (F) The stability of the electrochemical immunosensors at various storage periods.

Table 1
Assay results of clinical serum samples using the proposed and ELISA methods (n = 3).

Sample no.	Proposed method (ng mL^{-1})	ELISA (ng mL^{-1})	Relative deviation (%)
1	0.42 ± 0.048	0.40 ± 0.041	5.00
2	0.86 ± 0.084	0.81 ± 0.037	6.17
3	2.11 ± 0.11	2.03 ± 0.085	3.94
4	5.17 ± 0.09	5.39 ± 0.14	−4.08
5	9.74 ± 0.79	9.86 ± 0.67	−1.22
6	9.87 ± 0.78	10.49 ± 0.11	−5.91
7	10.11 ± 0.26	10.67 ± 0.49	−5.25
8	11.12 ± 0.47	10.79 ± 0.38	3.06
9	14.85 ± 0.13	15.03 ± 0.083	−1.20
10	15.88 ± 0.11	16.31 ± 0.55	−2.64

human serum samples. Table S2 displayed the results that the recovery was in the range of 93.3%–109.0%. Moreover, to address the reliability of our proposed immunosensors, the immunoassay of human serum samples with the proposed immunosensors were compared with those obtained by enzyme-linked immunosorbent assay (ELISA) as a reference method. As listed in Table 1, the relative errors between the two methods ranged from −5.91% to 6.17%, indicating an acceptable accuracy. These results indicated that the immunosensors are feasible and reliable for the detection of AFP in real clinical samples.

4. Conclusions

In summary, PIn-5-COOH prepared through a facile chemical method showed ultra-high redox stability. The current signal of CVs could remain 99.79% after 100 CV cycles and 96.03% even after 500 CV cycles. Besides the advantage of ultra-high redox stability, the PIn-5-COOH possesses one more advantage of abundant carboxyl functional group which can offer covalent binding sites with biomolecules in biosensors. Therefore, the PIn-5-COOH provides a promising platform for the construction of electrochemical sensors with ultra-stable redox signal. The electrochemical immunosensors based on PIn-5-COOH/MWCNTs-COOH nanocomposite showed ultra-stable redox signal, low detection limit, wide linear range, good selectivity, repeatability and long term stability. Our mechanism study indicated the ultra-high redox stability of PIn-5-COOH should be contributed to its structure stability. Nevertheless, to further understand why the structure of PIn-5-COOH is stable and origin of the difference in structure stability of PIn derivatives, quantum chemistry calculation of PIn derivatives is demanded for in-depth investigation in future work.

Declaration of interest statement

The authors declare that they have no known competing financial interests or personal relationships that could have appeared to influence the work reported in this paper.

CRediT authorship contribution statement

Taotao Yang: Conceptualization, Data curation, Formal analysis, Writing - original draft, Writing - review & editing. **Xiaoning Ren:** Formal analysis, Writing - review & editing. **Ming Yang:** Formal analysis, Writing - review & editing. **Xing Li:** Formal analysis. **Kaikai He:** Formal analysis. **Ai Rao:** Formal analysis. **Ying Wan:** Formal analysis. **Hai Yang:** Formal analysis. **Shenqi Wang:** Formal analysis. **Zhiqiang Luo:** Supervision, Writing - review & editing, Funding acquisition.

Acknowledgments

This work was supported by National Natural Science Foundation of China (No. 81771974).

Appendix A. Supplementary data

Supplementary data to this article can be found online at https://doi.org/10.1016/j.bios.2019.111406.

References

Ali, A.E., Zeinab, A., Mehdi, J., Rezaei, B., 2015. Electrochim. Acta 173, 619–629.
Dong, X.X., Yang, J.Y., Luo, L., Zhang, Y.F., Mao, C.B., Sun, Y.M., Lei, H.T., Shen, Y.D., Ross, C.B., Xu, Z.L., 2017. Biosens. Bioelectron. 98, 305–309.
Elena, C.M., Cao, Y., Kenneth, H.B., Christo, S.S., Miles, N.B., Brett, A.H., Jeffrey, S.M., Joaquín, R.L., 2018. Macromolecules 51, 3539–3546.
Gao, L.X., Teng, Y., 2016. Future Med. Chem. 8, 567–577.
Gao, Y.S., Xu, J.K., Lu, L.M., Zhu, X.F., Wang, W.M., Yang, T.T., Zhang, K.X., Yu, Y.F., 2015. RSC Adv. 5, 86910–86918.
Hedieh, H.H., Mohammad, M.H., Mohammad, R.S., Parviz, N., Mohammad, R.G., 2018. Sensor. Actuator. B Chem. 275, 61–68.
Heike, L.K.S.M., Stephanie, H., Renzo, M.P., Bernd, S., Ulrich, S.S., Anna, I., 2015. Phys. Chem. Chem. Phys. 17, 13323–13332.
Hu, Y.J., Hu, D.F., Ming, S.L., Duan, X.M., Zhao, F., Hou, J., Xu, J.K., Jiang, F.X., 2016. Electrochim. Acta 189, 64–73.
Jochen, K., Andreas, W., Hubert, F., Gerald, A.U., 2018. Lab Chip 18, 1274–1291.
Kashish, Dharmendra, K.S., Sunil, K.M., Rajiv, P., Suresh, K.D., 2015. J. Biotechnol. 200, 70–76.
Leela, J., Bhavana, G., Rajiv, P., 2010. Thin Solid Films 519, 218–222.
Li, X.M., Xia, J.P., Zhang, S.S., 2008. Anal. Chim. Acta 622, 104–110.
Li, R.X., Guo, D.Y., Ye, J.S., Zhang, M.N., 2015. Analyst 140, 3746–3752.
Li, Z.D., Li, F., Xing, Y., Liu, Z., You, M.L., Li, Y.C., Wen, T., Qu, Z.G., Li, X.L., Xu, F., 2017. Biosens. Bioelectron. 98, 478–485.
Liu, H.T., Zhen, S.J., Ming, S.L., Lin, K.W., Gu, H., Zhao, Y., Li, Y.Z., Lu, B.Y., Xu, J.K., 2016. J. Solid State Electrochem. 8, 2337–2349.
Luo, S.C., Sekine, J., Zhu, B., Zhao, H.C., Nakao, A., Yu, H.H., 2012. ACS Nano 6, 3018–3026.
Ma, X.M., Zhou, W.Q., Mo, D.Z., Hou, J., Xu, J.K., 2015. Electrochim. Acta 176, 1302–1312.
Maciejewska, J., Pisarek, K., Bartosiewicz, I., Krysinski, P., Jackowska, K., Biegunski, A.T., 2011. Electrochim. Acta 56, 3700–3706.
Mandira, M., Ram, B.C., Shankar, P.K., Anukul, K.T., Upendra, K., 2017. Electrochim. Acta 248, 98–111.
Mike, T., Yang, S.Y., Peng, S.J., Xu, Z., Shao, W.Y., Pan, D., Seeram, R., Zhu, M.F., 2017. Electrochim. Acta 247, 400–409.
Nie, G.M., Han, X.J., Hou, J., Zhang, S.S., 2007. J. Electroanal. Chem. 604, 125–132.
Nidhi, C., Jagriti, N., Pundir, C.S., 2011. Biosens. Bioelectron. 29, 82–88.
Niu, Y.L., Yang, T., Ma, S.S., Peng, F., Yi, M.H., Wan, M.M., Mao, C., Shen, J., 2017. Biosens. Bioelectron. 92, 1–7.
Qiu, J.D., Liang, R.P., Wang, R., Fan, L.X., Chen, Y.W., Xia, X.H., 2009. Biosens. Bioelectron. 25, 852–857.
Song, H.K., Palmore, G.T.R., 2006. Adv. Mater. 18, 1764–1768.
Utkarsh, J., Shaivya, G., Nidhi, C., 2017. Int. J. Biol. Macromol. 105, 549–555.
Wang, Z.W., Yang, H.K., Gao, B.W., Tong, Y., Zhang, X.J., Su, L., 2014. Analyst 139, 1127–1133.
Wang, Y.G., Zhang, Y., Wu, D., Ma, H.M., Pang, X.H., Fan, D.W., Wei, Q., Du, B., 2017. Sci. Rep. 7, 42361.
Xu, P., Han, X.J., Zhang, B., Du, Y.C., Wang, H.L., 2014. Chem. Soc. Rev. 43, 1349–1360.
Yang, T.T., Gao, Y.S., Liu, Z., Xu, J.K., Lu, L.M., Yu, Y.F., 2017. Sensor. Actuator. B Chem. 239, 76–84.
Yucel, S., Sabriye, P., Mutlu, S., Guleren, O., 2004. J. Appl. Polym. Sci. 91, 2302–2312.
Zhai, Q.F., Zhang, X.W., Li, J., Wang, E.K., 2016. Nanoscale 8, 15303–15308.
Zhang, W., 2016. J. Solid State Electrochem. 20, 499–506.
Zhang, D.D., Fu, L., Liao, L., Liu, N., Dai, B.Y., Zhang, C.X., 2012. Nano Res. 5, 875–887.
Zhang, Y.S., Aleman, J., Shin, S.R., Kilic, T., Kim, D., et al., 2017. Proc. Natl. Acad. Sci. U.S.A. 114, E2293–E2302.
Zhang, X.B., Li, Y.Y., Lv, H., Feng, J.H., Gao, Z.Q., Wang, Ping, Dong, Y.H., Liu, Q., Zhao, Z.D., 2018. Biosens. Bioelectron. 106, 142–148.
Zhao, Y., Liu, B.R., Pan, L.J., Yu, G.H., 2013. Energy Environ. Sci. 6, 2856–2870.